Research Square

Preprints are preliminary reports that have not undergone peer review.
They should not be considered conclusive, used to inform clinical practice,
or referenced by the media as validated information.

Reducing acid mine drainage potential in sulfide-rich tailings through selective sulfide removal: A case study from a polymetallic mine deposit in northeastern Türkiye

Selçuk Alemdağ
selcuk@gumushane.edu.tr
Gümüşhane University
Mehmet Ali Gücer
Gümüşhane University
İbrahim Çavuşoğlu
Gümüşhane University
Enver Akaryalı
Gümüşhane University
Halil İbrahim Zeybek
Ondokuz Mayıs University

Article

Keywords:

Posted Date: October 22nd, 2026

DOI: https://doi.org/10.21203/rs.3.rs-10989055/v1

License: This work is licensed under a Creative Commons Attribution 4.0 International License. Read Full License

Additional Declarations: No competing interests reported.

Abstract

Sulfide-rich mine tailings represent a major source of acid mine drainage (AMD) and associated metal mobilization. This study evaluates selective pyrite flotation as a source-control strategy for reducing the acid-generation potential of flotation tailings from a polymetallic Pb-Zn mine. Pyrite-rich flotation tailings (PRT) and desulfurized flotation tailings (FLT) were characterized by X-ray diffraction (XRD) and X-ray fluorescence (XRF), while their environmental behavior was assessed using short-term (72-h) contact leaching tests and acid-base accounting (ABA). Both tailings produced predominantly near-neutral leachates, with selective pyrite removal resulting in slightly higher pH values and generally lower mobility of several sulfide-associated elements. More importantly, total sulfur decreased from 10.6–14.7 wt.% in PRT to 0.8–1.8 wt.% in FLT, accompanied by a pronounced reduction in acid potential. Strongly negative net neutralization potential (NNP) values in PRT (− 299 to − 101 kg $CaCO_3$/t) shifted to positive values in FLT (107.8–148.4 kg $CaCO_3$/t), while neutralization potential ratios (NPR) increased from 0.35–0.69 to 2.95–6.82. XRD and XRF results further confirmed the reduction of sulfur-bearing phases following flotation. These results demonstrate that selective pyrite removal substantially reduces the AMD potential of sulfide-rich tailings and improves their geochemical stability, supporting safer storage and potential reuse within sustainable mine-waste management strategies.

1. Introduction

The growing global population, urbanization and demand for clean energy technologies are substantially increasing the need for critical metals, particularly copper (Cu) and zinc (Zn) [**1–2**]. Meeting this demand requires the continued expansion of mining activities. However, the progressive depletion of high-grade ore reserves has necessitated the exploitation of lower-grade ore reserves. This has substantially increased the amount of ore processed and, consequently, the volume of mine waste generated [**3**]. It is estimated that approximately 8–14 billion tons of mine waste are generated globally each year [**4**]. Over the next three decades, the cumulative amount of waste generated by copper mining alone is projected to reach 247 billion tones, approximately 2.3 times more than was generated before 2022 [**4**]. A significant proportion of this waste consists of fine-grained flotation tailings, which pose a considerable environmental risk due to their large volume and sulphide mineral content [**5–6**].

Among the environmental risks associated with sulfide-rich mine wastes, acid mine drainage (AMD) is recognized as one of the most serious and persistent environmental challenges. Although various sulfide minerals, including arsenopyrite, galena, chalcopyrite, pyrrhotite, and sphalerite, can contribute to AMD generation, pyrite is the most abundant and environmentally significant sulfide mineral, and its oxidation is widely recognized as the principal driver of AMD formation [**7–11**]. The presence of sulfide minerals alone is insufficient to generate AMD, water and oxygen are also required. Under oxidizing conditions, pyrite reacts with oxygen and water to produce sulfate (SO_4^{2-}), hydrogen ions (H^+), and ferrous iron (Fe^{2+}), as shown in Eq. (1) [**11**].

$$FeS_2 + 7/2O_2 + H_2O \rightarrow Fe^{2+} + 2SO_4^{2-} + 2H^+ \quad (1)$$

The H^+ ions released during pyrite oxidation lower the pH of surrounding waters, promoting the dissolution and mobility of potentially toxic metals from rocks and mine wastes [**12,13**]. In addition, Fe^{2+} is oxidized to Fe^{3+} (Eq. 2), which further oxidizes pyrite (Eq. 3), creating a self-sustaining cycle that accelerates AMD generation [**11**].

$$Fe^{2+} + 1/4O_2 + H^+ \rightarrow Fe^{3+} + 1/2H_2O \quad (2)$$

$$FeS_2 + 14Fe^{3+} + 8H_2O \rightarrow 15Fe^{2+} + 2SO_4^{2-} + 16H^+ \quad (3)$$

Environmental risks associated with pyrite-bearing mine wastes, particularly acid generation and metal mobilization, necessitate their effective management and safe disposal [**14**]. Among the available tailings management options, long-term storage in surface tailings storage facilities (TSFs) remains the most widely adopted practice worldwide [**15,16**]. Flotation tailings are typically transported as a slurry and stored in engineered TSFs for long-term or permanent containment [**17**].

Despite their widespread application, TSFs require the long-term physical and geochemical stability of large volumes of tailings during mine operation and after mine closure [**18**]. However, risks such as geotechnical instability, dam failure, seepage, and AMD generation have highlighted the need for more sustainable tailings management strategies [**5,19**]. One such approach is the reuse of tailings as cemented paste backfill (CPB), which reduces the volume of tailings requiring surface storage while simultaneously improving underground mine stability [**20**].

In addition to long-term storage in TSFs, the utilization of tailings as cemented paste backfill (CPB) has become an increasingly important strategy for sustainable mine waste management [**21**]. However, when sulfide-rich tailings are used, the presence of water and oxygen within the porous CPB matrix may promote sulfide oxidation, leading to acid generation, sulfate release, binder degradation, and reduced long-term durability [**22–25**]. In addition, groundwater infiltration during mine operation or after mine closure may further enhance sulfide oxidation and the release of potentially toxic elements, highlighting the importance of minimizing the acid-generating potential of tailings prior to their utilization in CPB applications [**22**].

One of the primary environmental concerns associated with both TSFs and CPB applications is acid generation caused by the oxidation of pyrite and other reactive sulfide minerals, together with the associated metal mobilization. Consequently, selective sulfide removal by flotation has emerged as an effective source-control strategy for reducing AMD generation and enabling safer management and reuse of mine tailings [**26–28**]. However, most previous studies have focused on desulfurization efficiency or sulfide recovery, whereas the long-term acid generation potential and environmental suitability of the resulting low-sulfur tailings remain largely unexplored.

In this study, sulfide-rich tailings collected from the mineral processing plant of a lead–zinc mine were subjected to selective pyrite removal by flotation, and the environmental performance of the resulting low-sulfur tailings was evaluated. The original and desulfurized tailings were characterized using mineralogical and geochemical analyses, while their acid generation potential and contaminant release behavior were assessed through static and leaching tests. Finally, the suitability of the desulfurized tailings for environmentally safer storage and potential reuse was evaluated, providing new insights into the effectiveness of selective sulfide removal as a source-control strategy for sustainable mine waste management.

2. Regional geology and mine characteristics

The study area is situated in the northern part of the Eastern Sakarya Zone, also referred to as the Eastern Pontide Orogenic Belt, in northeastern Türkiye. This tectonic unit represents a key segment of the Alpine-Himalayan orogenic system, which played a fundamental role in the geodynamic evolution of the region (Fig. 1a). The area is characterized by a wide range of magmatic rocks of varying composition and age, together with associated mineralization systems (**29**; Fig. 1b). The oldest lithological units comprise Early Carboniferous metamorphic rocks representing the Variscan basement (30), which are intruded by Middle-Late Carboniferous calc-alkaline plutonic rocks (31–35).

The pre-Jurassic basement is unconformably overlain by the Şenköy Formation, a volcano-sedimentary sequence including volcaniclastics and Ammonitico Rosso facies limestones (36). This unit is widely interpreted as a typical

rift-related deposit, reflecting sedimentation associated with transgressive conditions accompanied by intermittent volcanic activity. The Şenköy Formation begins with basal conglomerates composed of quartz and sandstone clasts, interbedded with coal-bearing levels, and is overlain by red, fossil-rich limestones of Ammonitico Rosso facies. Upsection, the sequence transitions into an alternation of volcanogenic conglomerate, sandstone, siltstone, and marl, locally intercalated with basic volcanic rocks such as tuff, tuffite, andesite, spilitic basalt, lava flows, and pyroclastics. This unit is conformably overlain by the Late Jurassic-Early Cretaceous Berdiga Formation, which consists predominantly of medium- to thick-bedded, locally massive limestones. The lower levels are characterized by dolomitic limestones, whereas the upper parts include intercalations of conglomerate, sandstone, and siltstone, culminating in limestone, dolomite, and dolomitic limestone.

During the Late Cretaceous, the Eastern Pontides display pronounced north-south lithological variations. In the northern zone, where the study area is located, intense magmatic activity resulted in the development of widespread volcanic and granitoid rocks. The most common units include the Çatak, Kızılkaya, Çağlayan, and Çayırbağ formations, which exhibit conformable relationships, along with the Upper Cretaceous-Paleocene Bakırköy Formation (**37**; Fig. 1b).

The Çatak Formation forms the basal unit of the study area and consists of basalt, andesite, and their pyroclastics, interbedded with clayey limestone, sandstone, and siltstone. It is overlain by the Kızılkaya Formation, composed of dacite, rhyolite, and associated pyroclastics, followed by the Çağlayan Formation, which includes basalt, andesite, and pyroclastic rocks. The Çayırbağ Formation, consisting of rhyolite, rhyodacite, and pyroclastics, overlies the Çağlayan Formation. These units are unconformably overlain by the Eocene Alibaba Formation, which begins with nummulitic limestones interbedded with sandstone and tuff, and upwardly grades into alternations of andesite, basalt, associated pyroclastics, basaltic-andesite agglomerate, lapilli tuff, and tuff. The sequence locally terminates with eroded levels of limestone, sandstone, marl, and tuff (37). All these units are intruded by the Kaçkar Granitoid. Granitoids that cut the Late Cretaceous units and are transgressively overlain by Early Middle Eocene rocks are defined as Kaçkar Granitoid I, whereas Eocene intrusive rocks are referred to as Kaçkar Granitoid II (37).

The Eastern Black Sea region constitutes a significant segment of the Alpine-Himalayan metallogenic belt and is notable for hosting diverse economically important mineralization types. These include volcanogenic massive sulfide (VMS) deposits, skarn and porphyry-type Cu-Au-Mo systems, and skarn- and epithermal vein-type Cu, Pb, Zn, Au, and Ag mineralizations (37–47). These mineralizations are predominantly associated with volcanic rocks that are widely exposed, particularly in the Gümüşhane-Giresun region (48–51).

The mineralization in the study area is genetically related to the emplacement of the Upper Cretaceous (Campanian-Maastrichtian) Harşit Granitoid, which intrudes volcanic-sedimentary rocks previously described as the Pontide Lower Basic Complex (52). Although this volcano-sedimentary sequence was defined as the Çatak Formation in the Değirmendere Valley (Trabzon) by (37), within the study area it corresponds to the Çatak, Kızılkaya, and Çağlayan formations (Fig. 1b). Mineralization is mainly hosted by dacitic rocks, although other lithologies such as andesite, epiclastic units (claystone and sandstone), limestone, mudstone, agglomerate, tuff, and diabase are also present. Alteration is widespread, with kaolinization being the dominant type. Additionally, skarn-type mineralization occurs locally at contacts between intrusive rocks and carbonate units.

Microscopic investigations of ore samples collected from galleries, veins, and mine dumps indicate that mineralization developed in two distinct stages, followed by evidence of contact metamorphism (Fig. 2). The paragenetic assemblage comprises pyrite, sphalerite, chalcopyrite, and magnetite, accompanied by quartz, calcite, epidote, and garnet. Following the first mineralization stage, fracturing events resulted in the development of

cataclastic textures, with replacement processes playing a significant role. After the second stage, deformation continued with the formation of dissociation textures, along with ongoing replacement and fracturing.

Pyrite, readily identifiable by its metallic yellow color in polished sections, represents the earliest ore mineral and commonly occurs in association with chalcopyrite, sphalerite, and quartz (Fig. 2). Sphalerite typically occurs as coarse, irregularly shaped crystals with broad surfaces, as well as smaller crystals exhibiting grey to light grey tones, and shows a close paragenetic relationship with chalcopyrite. Textural evidence indicates mutual replacement between sphalerite and chalcopyrite, as well as the presence of chalcopyrite disease textures reflecting co-precipitation. Magnetite, generally displaying anhedral and fractured textures, is interpreted to have formed during the second stage. It is partially replaced by gangue minerals and subsequently altered to hematite during later alteration processes (Fig. 2).

3. Materials and methods

To evaluate the environmental benefits of selective pyrite removal, the original sulphide-rich tailings (To) and the desulfurized tailings (Tf) underwent thorough characterization, including geochemical analyses, static acid–base accounting (ABA) and short-term contact leaching tests. The resulting leachates were then evaluated against relevant water quality standards and characteristic mine drainage compositions to assess changes in acid-generation potential and contaminant release, as well as the overall environmental suitability of the desulfurized tailings. Detailed descriptions of the analytical procedures are provided below.

3.1. Sampling

Ore-bearing and host rock samples, drill cores, and flotation tailings were collected during the field investigation (Fig. 3). However, the present study focuses exclusively on flotation tailings generated during the ore processing of a polymetallic Pb-Zn-Cu mine. The investigated tailings consisted of two materials collected from the flotation circuit: (i) pyrite-rich flotation tailings (PRT) produced prior to pyrite separation and (ii) desulfurized flotation (pyrite flotation) tailings (FLT) obtained after selective pyrite removal. These samples constituted the dataset used for all subsequent mineralogical, geochemical, acid–base accounting (ABA) and leaching analyses. The dataset analyzed comprised 15 samples, including 10 PRT and 5 FLT samples. The PRT samples represent sulfide-rich tailings with high acid-generating potential, whereas the FLT samples represent desulfurized tailings with substantially reduced sulfide contents following pyrite removal.

3.2. Contact leaching tests

Short-term contact leaching tests were performed on PRT and FLT using a modified US EPA Method 1312 protocol. Samples were mixed with deionized water at a liquid-to-solid ratio of 3:1 and agitated on a digital orbital shaker at 300 rpm for 72 h. Following agitation, the suspensions were filtered and the pH of the leachates was measured. For elemental analysis, aliquots were acidified with 2% HNO_3 prepared from 65% suprapur HNO_3 and filtered through 0.45 µm membranes. Where required, samples were diluted 4-20-fold prior to analysis. Concentrations of Mg, Al, Ca, Cr, Mn, Fe, Co, Ni, Cu, Zn, Cd, and Pb were determined using an Agilent 7700 ICP-MS at the Gümüşhane University Central Research Laboratory (GÜ-MERLAB). The resulting leachate compositions were subsequently used to evaluate metal release behavior and were compared with relevant water-quality criteria.

3.3. Acid–base accounting (ABA) tests

Acid-base accounting (ABA) tests were performed on PRT and FLT to evaluate changes in acid generation potential following selective pyrite removal. The analyses were conducted by Düzen Norwest Environmental, Food and Veterinary Health Services, Training and Consultancy Inc. (Ankara, Türkiye). Paste pH, total sulfur, sulfate, carbonate, sulfide sulfur, and neutralization potential (NP) were determined using standardized analytical procedures, including ISO 10390, TS EN 12879, EPA 3051A/EPA 6010D, EPA 9056A, TS EN ISO 10693, and TS EN 12457-4. Acid potential (AP) was calculated from the sulfide-sulfur content as Total S (%)×31.25. Neutralization potential was determined by acid digestion followed by back-titration with NaOH to pH 8.33. The resulting AP and NP values were used to calculate net neutralization potential (NNP = NP-AP) and the neutralization potential ratio (NPR = NP/AP). These parameters, together with paste pH and sulfide-sulfur contents, were used to classify the acid-generating characteristics of the original and desulfurized tailings and to quantify the effect of selective pyrite removal on AMD potential.

3.4. X-ray diffraction (XRD) and X-ray fluorescence (XRF) analysis

The mineralogical compositions of the PRT and FLT were determined by X-ray diffraction (XRD). Prior to analysis, the samples were oven-dried, homogenized, and pulverized to obtain fine powders. XRD measurements were performed using a PANalytical Empyrean diffractometer equipped with a Cu anode X-ray tube and a 256×256-pixel detector. Cu Kα radiation (λ = 1.5406 Å) was used, and diffraction patterns were recorded over a 2θ range of 5–70°. Mineral phases were identified by comparison of the measured diffraction patterns with reference patterns in the crystallographic database used for phase identification. The bulk chemical compositions of the PRT and FLT were determined using a PANalytical Zetium X-ray fluorescence (XRF) spectrometer. Prior to analysis, the samples were dried, ground, and homogenized. The chemical compositions were reported as oxide concentrations in weight percent (wt.%), including both major and minor components. Loss on ignition (LOI) was also determined and reported as wt.%.

3.5. Selective pyrite flotation process

Selective pyrite removal from the PRT was performed using a two-stage laboratory-scale flotation process consisting of rougher and cleaner stages (Fig. 4a). A representative laboratory-scale flotation experiment is shown in Fig. 4b. Process recycle water collected from the same mineral processing plant was used for pulp preparation to preserve, as far as practicable, the physicochemical characteristics of the industrial water circuit. Prior to rougher flotation, the slurry pH was adjusted to 6.0 using dilute H_2SO_4. Potassium amyl xanthate (PAX) and methyl isobutyl carbinol (MIBC) were added at dosages of 450 and 25 g/t, respectively, as collector and frother, and rougher flotation was conducted for 8 min. The pyrite-rich rougher concentrate was subsequently subjected to cleaner flotation, whereas the non-floated fraction was collected as desulfurized rougher tailings. Before cleaner flotation, the slurry pH was readjusted to 6.0 using dilute H_2SO_4. Sodium silicate (Na_2SiO_3; 300 g/t) was added as a depressant/dispersant, followed by PAX at 200 g/t. No additional MIBC was used during this stage. Cleaner flotation was performed for 6 min, producing a final pyrite concentrate and a cleaner tailings fraction. The cleaner tailings were combined with the non-floated rougher tailings to constitute the final FLT used in the subsequent analyses.

4. Results and discussion

4.1. Assessment of contact leaching tests

The results of the short-term (72-h) contact leaching tests conducted to evaluate the release of dissolved constituents from the PRT and FLT are summarized in Table 1. The resulting leachate compositions were also evaluated against the surface-water quality classes defined in (53).

The PRT samples produced predominantly near-neutral leachates, with pH values ranging from 6.45 to 6.89 (mean = 6.73), whereas the FLT samples exhibited slightly higher pH values of 7.01–7.25 (mean = 7.14) (Table 1). Thus, selective pyrite removal increased the mean leachate pH by approximately 0.4 units, indicating a shift toward slightly more alkaline conditions. The near-neutral pH values observed in both groups indicate that no short-term acidification developed during the 72-h contact period, while the higher pH values of the FLT leachates suggest a reduced tendency toward acidification following desulfurization.

The contact leaching results also revealed marked differences in elemental mobility between the PRT and FLT samples (Table 1). Al, Cr, Fe, As, and Pb remained below the limit of quantification (LOQ) in both groups, indicating negligible short-term release of these elements under the experimental conditions. Among the potentially toxic elements, Mn and Zn showed the highest dissolved concentrations, whereas Co, Ni, Cu, and Cd were generally released at much lower levels. Mn concentrations ranged from 3.19 to 5.05 mg/L in the PRT leachates and increased to 7.50–8.62 mg/L following pyrite removal, whereas Zn decreased markedly from 0.70–1.19 mg/L in PRT to 0.01–0.26 mg/L in FLT. Similar decreases were observed for Co and Cd, while Cu showed a relative increase in the FLT leachates, although its concentrations remained substantially lower than those of Mn. These contrasting trends indicate that selective pyrite removal substantially reduced the mobility of some sulfide-associated elements, particularly Zn, Co, and Cd, but did not uniformly decrease the release of all elements.

4.2. Water-quality assessment of the leachates

The environmental significance of the leachate compositions was evaluated by comparison with the surface-water quality classes defined in RG 28483 (53) and the drinking-water guideline values of TS266, WHO, USEPA, and EC (Table 1).

Table 1
Element concentrations in PRT and FLT leachates obtained from contact leaching tests and comparison with selected water-quality criteria (mg/L)

TS266[a]	**pH (20°C)**	**Al**	**Cd**	**Co**	**Cr**	**Cu**	**Fe**	**Mn**	**Ni**	**Pb**	**Zn**
	6.5–9.5	**0.2**	**0.005**	**0.05**	**0.05**	**2**	**0.2**	**0.05**	**0.02**	**0.01**	**5**
WHO[b]	6.5-8.0	0.1	0.003	Ø	0.05	2	0.3	0.1	0.02	0.01	3
USEPA[c]	6.5–8.5	0.2	0.005	Ø	0.1	1	0.3	0.05	Ø	0.015	5
EC[d]	6.5–9.5	Ø	0.005	Ø	0.05	2	0.2	0.05	Ø	0.01	Ø
Quality Classification of the Intra-Continental Water Resources*											
I	6.5–8.5	≤ 0.3	≤ 0.002	≤ 0.01	≤ 0.02	≤ 0.02	≤ 0.3	≤ 0.1	≤ 0.02	≤ 0.01	≤ 0.2
II	6.5–8.5	≤ 0.3	0.005	0.02	0.05	0.05	1	0.5	0.05	0.02	0.5
III	6.0–9.0	1	0.007	0.2	0.2	0.2	5	3	0.2	0.05	2
IV	< 6.0 or > 9.0	> 1	> 0.007	> 0.2	> 0.2	> 0.2	> 5	> 3	> 0.2	> 0.05	> 2
Samples	**PRT tailings**										
ALG 1T	6.86	LOQ	0.0048	0.0046	LOQ	0.0006	LOQ	**5.05**	0.010	LOQ	1.19
ALG 2T	6.45	LOQ	0.0037	0.0044	LOQ	0.0005	LOQ	**4.33**	0.012	LOQ	1.06
ALG 3T	6.87	LOQ	0.0035	0.0036	LOQ	0.0003	LOQ	**3.65**	0.008	LOQ	0.90
ALG 4T	6.82	LOQ	0.0035	0.0033	LOQ	0.0002	LOQ	**3.27**	0.007	LOQ	0.91
ALG 5T	6.64	LOQ	0.0032	0.0034	LOQ	0.0003	LOQ	**3.39**	0.008	LOQ	0.86
ALG 6T	6.69	LOQ	0.0034	0.0036	LOQ	0.0001	LOQ	**3.31**	0.009	LOQ	0.93
ALG 7T	6.77	LOQ	0.0040	0.0042	LOQ	0.0004	LOQ	**4.29**	0.012	LOQ	1.08
ALG 8T	6.77	LOQ	0.0040	0.0042	LOQ	0.0001	LOQ	**4.32**	0.011	LOQ	0.99
ALG 9T	6.89	LOQ	0.0035	0.0035	LOQ	0.0001	LOQ	**3.47**	0.007	LOQ	0.85
ALG 10T	6.58	LOQ	0.0037	0.0028	LOQ	0.0015	LOQ	**3.19**	0.007	LOQ	0.70
	FLT tailings										
ALG 1PS	7.07	LOQ	0.0010	0.0005	LOQ	0.0624	LOQ	**7.50**	0.020	LOQ	0.26

*Regulation on Surface Water Quality Management, the Turkish Standards, 30.11.2012, number 28483 (revision: RG-15.4.2015–29327). LOQ: Limit of Quantitation, 0.25 mg/L for Ca and Mg, and 0.01 mg/L for other elements. Elements that leach into the water in high concentrations upon contact are shown in bold. PRT waste: Pyrite flotation waste, and FLT waste: Represents waste samples after pyrite (desulfurized) flotation. a: Turkish Standards (TS266, 2005), b: World Health Organization, c: United States Environmental Protection Agency, d: European Community indicate the permitted maximum values.

TS266[a]	pH (20°C)	Al	Cd	Co	Cr	Cu	Fe	Mn	Ni	Pb	Zn
	6.5–9.5	**0.2**	**0.005**	**0.05**	**0.05**	**2**	**0.2**	**0.05**	**0.02**	**0.01**	**5**
ALG 2PS	7.01	LOQ	0.0010	0.0003	LOQ	0.0107	LOQ	**8.28**	LOQ	LOQ	0.01
ALG 3PS	7.16	LOQ	0.0010	0.0003	LOQ	0.0156	LOQ	**8.62**	LOQ	LOQ	0.05
ALG 4PS	7.22	LOQ	0.0010	0.0004	LOQ	0.0171	LOQ	**8.33**	0.002	LOQ	0.07
ALG 5PS	7.25	LOQ	0.0009	0.0003	LOQ	0.0052	LOQ	**7.76**	LOQ	LOQ	0.01

*Regulation on Surface Water Quality Management, the Turkish Standards, 30.11.2012, number 28483 (revision: RG-15.4.2015–29327). LOQ: Limit of Quantitation, 0.25 mg/L for Ca and Mg, and 0.01 mg/L for other elements. Elements that leach into the water in high concentrations upon contact are shown in bold. PRT waste: Pyrite flotation waste, and FLT waste: Represents waste samples after pyrite (desulfurized) flotation. a: Turkish Standards (TS266, 2005), b: World Health Organization, c: United States Environmental Protection Agency, d: European Community indicate the permitted maximum values.

The pH values of all FLT leachates and all but one PRT sample (ALG2T; pH = 6.45) fell within the generally accepted range of 6.5–8.5/9.5, confirming the predominantly near-neutral character of the leachates. In contrast, Mn represented the principal water-quality concern, with concentrations of 3.19–5.05 mg/L in PRT and 7.50–8.62 mg/L in FLT, substantially exceeding the relevant guideline values. Most other potentially toxic elements remained within the respective drinking-water limits or below the limit of quantification. The distribution of selected potentially toxic metals relative to the TS266 maximum acceptable limits is illustrated in Fig. 5. However, some element-specific differences were evident: Zn concentrations in PRT leachates exceeded the Class II surface-water criterion but remained below drinking-water limits, while Cd in PRT exceeded the WHO guideline value although remaining below the TS266, USEPA, and EC limits. Overall, the results indicate that Mn, rather than generalized metal release, is the dominant short-term water-quality constraint for both tailing types.

Beyond the regulatory comparison, the leachate chemistry was also evaluated in terms of its general mine-drainage characteristics. The PRT leachates correspond predominantly to a near-neutral/low-metal drainage type, characterized by near-neutral pH, moderate Zn concentrations, and generally low concentrations of Cu, Fe, Al, Cd, and Ni. Following selective pyrite removal, the FLT leachates shifted toward a more buffered/low-metal drainage character, with slightly higher pH and markedly lower concentrations of Zn and other sulfide-associated metals. This shift indicates that desulfurization improved the overall short-term drainage quality by reducing the mobility of several metal contaminants. However, the persistence and increase of Mn in the FLT leachates demonstrate that selective pyrite removal did not uniformly decrease the release of all dissolved constituents.

The mine-drainage characteristics of the leachates were further evaluated using the Ficklin geochemical classification diagrams, in which the sum of dissolved base metals (Zn + Cu + Cd + Pb + Co + Ni) is plotted against pH (54–56). Both PRT and FLT leachates plot within the Neutral Mine Drainage field and predominantly occupy the near-neutral/low-metal domain (Fig. 6). However, the PRT samples display systematically higher total base-metal concentrations than the FLT samples, indicating a shift toward lower-metal drainage conditions following selective pyrite removal. In the process-control diagram, the samples show trends broadly consistent with increasing dilution by surface water and decreasing carbonate influence, while the PRT samples remain relatively closer to the higher-metal side of the distribution (Fig. 6). Overall, the Ficklin classification supports the contact-leaching results by showing that selective pyrite removal reduces the short-term dissolved base-metal load of the tailings without producing acidic drainage under the tested conditions.

4.3. Assessment of acid-base accounting (ABA)

The acid–base accounting (ABA) results for the PRT and FLT are summarized in Table 2. Paste pH values ranged from 7.9 to 8.0 in the PRT samples and from 7.5 to 8.7 in the FLT samples, indicating neutral to alkaline conditions in both groups. According to commonly used static-test criteria, paste pH values above 7 generally indicate a low tendency for acid generation (57). However, paste pH alone does not adequately represent the balance between acid-generating and acid-neutralizing components of mine wastes. More importantly, total sulfur contents decreased markedly from 10.6–14.7 wt.% (mean = 12.86 wt.%) in PRT to 0.8–1.8 wt.% (mean = 1.44 wt.%) in FLT following selective pyrite flotation. This corresponds to an approximately 89% decrease in mean total sulfur content and demonstrates the effective removal of sulfur-bearing phases during desulfurization. Accordingly, the acid-generation characteristics of the tailings were further evaluated using acid potential (AP), neutralization potential (NP), net neutralization potential (NNP), and neutralization potential ratio (NPR).

Table 2
Acid–base accounting (ABA) parameters and calculated acid-generation indices for pyrite-rich (PRT) and desulfurized (FLT) tailings.

Unit	Paste pH	TIC[1]	Carbonate ($CaCO_3$)	Sulphur (Total S)	Sulphide (S^{2-})	Sulfate (SO_4^{2-})	NP[2]	AP[3]	NNP[4]	NPR[5]
	–	wt.%	wt.%	wt.%	wt.%	wt.%	kg/t $CaCO_3$	kg/t $CaCO_3$	kg/t $CaCO_3$	–
Samples	**PRT tailings**									
ALG-1	8.0	93.3	12.4	10.6	0.9	0.3	213	331	-119	0.64
ALG-2	8.0	93.0	12.2	14.0	1.0	0.3	165	438	-273	0.38
ALG-3	8.0	93.3	12.7	14.2	0.9	0.4	213	444	-231	0.48
ALG-4	7.9	93.3	12.1	14.7	1.2	0.4	160	459	-299	0.35
ALG-5	8.0	93.1	13.0	10.6	0.7	0.3	230	331	-101	0.69
ALG-6	8.0	92.5	11.9	13.9	1.8	0.2	218	434	-216	0.50
ALG-7	8.0	93.5	11.6	11.0	0.9	0.5	201	344	-143	0.59
ALG-8	8.0	93.2	12.2	12.6	0.9	0.4	179	394	-214	0.46
ALG-9	8.0	93.5	11.4	13.5	1.0	0.4	211	422	-211	0.50
ALG-10	8.0	92.7	11.4	13.5	0.9	0.4	213	422	-209	0.51
	FLT tailings									
ALG-1PS	8.0	96.5	12.3	1.8	< 1	0.3	163.1	55.3	107.8	2.95
ALG-2PS	7.5	96.8	14.1	1.8	< 1	1.1	199.4	54.7	144.7	3.65
ALG-3PS	8.7	96.1	12.8	1.6	< 1	0.1	176.2	50.6	125.6	3.48
ALG-4PS	7.8	96.6	12.1	0.8	< 1	1.4	164.4	24.1	140.3	6.82
ALG-5PS	7.7	96.5	13.0	1.2	< 1	0.9	187.5	39.1	148.4	4.80

[1]TIC (%): Total incombustible content. [2]NP: Neutralization potential determined by titration (60). [3]AP: Acid potential calculated from total sulfur content (AP = Total S × 31.25) (60). [4]NNP: Net neutralization potential (NNP = NP − AP). [5]NPR: Neutralization potential ratio (NPR = NP/AP)

Acid potential showed a pronounced decrease following selective pyrite removal. Based on the laboratory calculation procedure (AP = total S × 31.25), AP values ranged from 331 to 459 kg $CaCO_3$/t in the PRT samples but decreased to 24.1–55.3 kg $CaCO_3$/t in the FLT samples (Table 2), corresponding to an approximately 89% reduction in mean AP. In contrast, NP remained comparatively high in both groups, ranging from 160 to 230 kg $CaCO_3$/t in PRT and from 163.1 to 199.4 kg $CaCO_3$/t in FLT. Consequently, NNP values shifted from strongly negative values of − 299 to − 101 kg

$CaCO_3$/t in PRT to strongly positive values of 107.8–148.4 kg $CaCO_3$/t in FLT. According to the widely used criterion of (58), materials with NNP < − 20 kg $CaCO_3$/t are considered potentially acid-generating, whereas those with NNP > + 20 kg $CaCO_3$/t are classified as non-acid-generating. Accordingly, all PRT samples plot within the acid-generating field, whereas all FLT samples plot well within the non-acid-generating field (Fig. 7a). This marked reversal in NNP demonstrates that selective pyrite removal substantially altered the balance between acid production and neutralization in favor of net neutralization.

A similar distinction is evident from NPR values, which express the ratio of neutralization potential to acid potential (NP/AP). Brodie et al (59) proposed NPR < 1 for acid-generating materials, NPR > 3 for non-acid-generating materials, and values between 1 and 3 as an uncertain range for which further kinetic evaluation may be required. The PRT samples yielded consistently low NPR values of 0.35–0.69 (mean = 0.51), confirming their strong acid-generating character (Fig. 7b). In contrast, NPR values increased to 2.95–6.82 (mean = 4.34) after selective pyrite removal. Four of the five FLT samples exceeded the NPR = 3 non-acid-generating thresholds, whereas one sample (ALG-1PS; NPR = 2.95) plotted immediately below this boundary. Notably, this borderline sample still exhibited a strongly positive NNP of 107.8 kg $CaCO_3$/t, indicating substantial excess neutralization capacity. Thus, when NNP and NPR are considered together, the FLT samples show a pronounced transition from acid-generating to predominantly non-acid-generating behavior following desulfurization.

Collectively, the ABA results provide strong evidence that selective pyrite flotation substantially reduces the intrinsic acid-generation potential of the tailings. Although paste pH remained near-neutral to alkaline in both PRT and FLT samples, the untreated PRT samples retained high sulfur contents, high AP values, strongly negative NNP values, and NPR values consistently below 1, all of which indicate a considerable potential for future acid generation. Following desulfurization, the marked reduction in sulfur and AP, combined with persistently high NP, resulted in strongly positive NNP values and predominantly NPR > 3. These results demonstrate that the environmental benefit of pyrite removal is not simply reflected by short-term pH conditions but, more importantly, by a fundamental shift in the balance between acid-producing and neutralizing components. Together with the contact-leaching results, the ABA data therefore indicate that selective pyrite removal can substantially improve the geochemical stability of sulfide-rich tailings and reduce their potential to generate AMD during subsequent storage or reuse.

4.4. Mineralogical and geochemical characterization of the tailings

XRD analyses revealed clear mineralogical differences between the PRT and FLT samples (Fig. 8). The PRT sample is characterized mainly by quartz, pyrite, clinochlore, albite, gypsum, and bassanite, with distinct pyrite reflections confirming the presence of sulfide-bearing phases (Fig. 8a). Under oxidizing conditions, pyrite can generate sulfate and acidity through its reaction with oxygen and water. Thereby promoting a decrease in pH and potentially enhancing metal mobility. The occurrence of gypsum and bassanite further indicates the presence of sulfate-bearing phases and may reflect previous or ongoing sulfide oxidation. In contrast, the FLT sample contains quartz and residual pyrite together with magnesium calcite, corundophilite, willhendersonite, clinoenstatite, amesite-2A, and albite (Fig. 8b). Although pyrite was not completely removed, magnesium calcite may contribute to acid neutralization, while the associated silicate minerals may provide additional buffering capacity during longer-term water–rock interaction. This mineralogical contrast is consistent with the lower acid-generation tendency and greater neutralization capacity of the FLT material indicated by the ABA results.

The XRF data supports the mineralogical differences observed by XRD (Table 3). The PRT sample is dominated by SiO_2 (43.72 wt.%), Fe_2O_3 (14.20 wt.%), CaO (10.38 wt.%), Al_2O_3 (9.39 wt.%), and MgO (7.97 wt.%), whereas the FLT

sample contains 34.45 wt.% SiO_2, 15.53 wt.% Fe_2O_3, 8.71 wt.% Al_2O_3, 7.63 wt.% CaO, and 7.42 wt.% MgO. More importantly, SO_3 decreases from 3.72 wt.% in PRT to 1.23 wt.% in FLT, corresponding to an approximately 67% reduction following selective pyrite flotation. This decrease is consistent with the removal of sulfur-bearing phases and with the lower total sulfur and acid potential determined by ABA. The substantially higher loss on ignition of the FLT sample (22.14 wt.%, compared with 7.18 wt.% in PRT) may reflect a greater contribution from volatile-bearing, hydrated, and/or carbonate phases, although LOI alone cannot uniquely identify their mineralogical source. Taken together, the XRD and XRF results indicate that selective pyrite removal produced a clear mineralogical and chemical modification of the tailings toward a composition with lower sulfur content and potentially greater geochemical stability.

Table 3
XRF-determined chemical compositions of PRT and FLT tailings (wt.%)

Component	PRT Tailings	FLT Tailings	Component	PRT Tailings	FLT Tailings
Fe_2O_3	14.199	15.528	PbO	0.014	0.011
SiO_2	43.718	34.450	CuO	0.014	0.023
Al_2O_3	9.392	8.714	NiO	0.002	0.003
CaO	10.376	7.631	Cr_2O_3	0.037	0.041
MgO	7.972	7.424	V_2O_5	0.016	0.016
Mn_3O_4	1.146	0.966	BaO	0.007	0.010
SO_3	3.717	1.230	P_2O_5	0.089	0.070
Na_2O	1.003	0.843	ZrO_2	0.002	0.002
K_2O	0.603	0.508	SrO	0.012	0.010
TiO_2	0.344	0.274	LOI	7.177	22.140
ZnO	0.162	0.111			

Conclusion

Selective pyrite flotation substantially modified the geochemical and environmental behavior of the sulfide-rich tailings investigated in this study. The short-term contact leaching tests showed that both PRT and FLT produced predominantly near-neutral leachates, while desulfurization shifted the pH toward slightly more alkaline conditions. Selective pyrite removal markedly reduced the short-term mobility of several sulfide-associated elements, particularly Zn, Co, and Cd. However, Mn remained the principal water-quality concern and showed higher concentrations in the FLT leachates. Ficklin classification further indicated that both tailing types exhibited near-neutral/low-metal drainage characteristics under the tested conditions, with FLT showing a clear shift toward lower dissolved base-metal loads.

The ABA results provided the strongest evidence of reduced acid-generation potential following desulfurization. Total sulfur decreased from 10.6–14.7 wt.% in PRT to 0.8–1.8 wt.% in FLT, accompanied by a pronounced decrease in acid potential. Accordingly, strongly negative NNP values in PRT changed to strongly positive values in FLT, while NPR increased from consistently acid-generating values below 1 to predominantly non-acid-generating values around or

above 3. These results demonstrate that selective pyrite removal substantially shifts the acid–base balance of the tailings toward net neutralization.

The mineralogical and chemical data support these findings. XRD and XRF results indicate a marked reduction in sulfur-bearing phases after flotation, together with the persistence of carbonate- and silicate-bearing phases capable of contributing to buffering reactions. The decrease in SO_3 from 3.72 wt.% in PRT to 1.23 wt.% in FLT is consistent with the reduction in total sulfur and acid potential determined by ABA. Collectively, the results show that selective pyrite flotation can substantially reduce the AMD potential of sulfide-rich tailings and improve their geochemical stability, thereby supporting their safer storage and potential reuse in sustainable mine-waste management applications.

Declarations

Acknowledgements

The authors gratefully acknowledge Alagöz Maden San. Tic. A.Ş. for providing access to the mine site, logistical support during field investigations and sample collection, and assistance throughout the fieldwork. The authors also thank the company for supporting the analytical work carried out within the scope of this study.

Funding

This study received financial support from Alagöz Maden San. Tic. A.Ş., including support for field activities, sample collection, and analytical costs.

Author contributions

Alemdağ, S.: Conceptualization, Methodology, Validation, Investigation, Data curation, Writing-original draft, Writing-review & editing, Supervision, Project administration, Funding acquisition. **Gücer, M. A.:** Conceptualization, Methodology, Software, Validation, Investigation, Data curation, Writing-original draft, Writing-review & editing, Visualization. **Çavuşoğlu, İ.:** Conceptualization, Methodology, Software, Validation, Investigation, Data curation, Writing-original draft, Writing-review & editing, Visualization. **Akaryalı, E.:** Conceptualization, Methodology, Validation, Investigation, Data curation, Writing-original draft, Writing-review & editing, Visualization. **Zeybek, H. İ.**: Investigation, Resources, Writing-review & editing.

Competing interests

The authors declare no competing interests.

Data availability

The data supporting the findings of this study are included in the article. Additional data generated and/or analyzed during the current study are available from the corresponding author on reasonable request.

References

1. Elshkaki, A., Graedel, T. E., Ciacci, L. & Reck, B. Copper demand, supply, and associated energy use to 2050. *Glob Environ. Change*. **39**, 305–315. https://doi.org/10.1016/j.gloenvcha.2016.06.006 (2016).

2. World Bank. The Growing Role of Minerals and Metals for a Low Carbon Future. World Bank, (2017). https://openknowledge.worldbank.org/entities/publication/4cdae3a6-3244-56e5-9de3-8faa5b6c88da
3. Guo, D. et al. Global copper tailings distribution and projection. *Nat. Sustain.* **9**, 774–782. https://doi.org/10.1038/s41893-026-01795-x (2026).
4. Franks, D. M. et al. Lessons from tailings facility data disclosures. In Towards Zero Harm: A Compendium of Papers Prepared for the Global Tailings Review (eds Oberle, B., Brereton, D. & Mihaylova, A.) 84–108 (Global Tailings Review, 2020).
5. Tomiyama, S., Igarashi, T., Tabelin, C. B., Tangviroon, P. & Ii, H. Acid mine drainage sources and hydrogeochemistry at the Yatani mine, Yamagata, Japan: A geochemical and isotopic study. *J. Contam. Hydrol.* **225**, 103502. https://doi.org/10.1016/j.jconhyd.2019.103502 (2019).
6. Araujo, F. S. M., Taborda-Llano, I., Nunes, E. B. & Santos, R. M. Recycling and reuse of mine tailings: A review of advancements and their implications. *Geosciences* **12**, 319. https://doi.org/10.3390/geosciences12090319 (2022).
7. Park, I. et al. A review of recent strategies for acid mine drainage prevention and mine tailings recycling. *Chemosphere* **219**, 588–606. https://doi.org/10.1016/j.chemosphere.2018.11.053 (2019).
8. Tu, Z. et al. Reduction of acid mine drainage by passivation of pyrite surfaces: A review. *Sci. Total Environ.* **832**, 155116. https://doi.org/10.1016/j.scitotenv.2022.155116 (2022).
9. Alemdag, S., Akaryalı, E. & Gücer, M. A. Prediction of mine drainage generation potential and the prevention method in the Gümüşköy (Kütahya) mineralization area, NW-Turkey. *J. Mt. Sci.* **17**, 2387–2404. https://doi.org/10.1007/s11629-020-6124-1 (2020).
10. Gücer, M. A., Alemdağ, S. & Akaryalı, E. Assessment of acid mine drainage formation using geochemical and static tests in Mutki (Bitlis, SE Turkey) mineralization area. *Turk. J. Earth Sci.* **29**, 1189–1210. https://doi.org/10.3906/yer-2002-18 (2020).
11. Akcil, A. & Koldas, S. Acid mine drainage (AMD): Causes, treatment and case studies. *J. Clean. Prod.* **14**, 1139–1145 (2006).
12. Miracle, O., Fall, M. & Ghirian, A. Flow characteristics of paste tailings in surface disposal: The role of pyrite content. *Environ. Sci. Pollut Res.* **32**, 6446–6467. https://doi.org/10.1007/s11356-025-36051-w (2025).
13. Simate, G. S. & Ndlovu, S. Acid mine drainage: Challenges and opportunities. *J. Environ. Chem. Eng.* **2**, 1785–1803. https://doi.org/10.1016/j.jece.2014.07.021 (2014).
14. Dold, B. IntechOpen,. Basic concepts in environmental geochemistry of sulfidic mine-waste management. In Waste Management (ed. Kumar, S.) 173–198 (2010).
15. Blight, G. Mine waste: A brief overview of origins, quantities, and methods of storage. In Waste: A Handbook for Management (eds (eds Letcher, T. M. & Vallero, D. A.) 77–88 (Academic, (2011).
16. Franks, D. M., Boger, D. V., Cote, C. M. & Mulligan, D. R. Sustainable development principles for the disposal of mining and mineral processing wastes. *Resour. Policy*. **36**, 114–122. https://doi.org/10.1016/j.resourpol.2010.12.001 (2011).
17. Dixon-Hardy, D. & Engels, J. Methods for the disposal and storage of mine tailings. *Land. Contam. Reclam.* **15**, 301–317 (2007).
18. Ayres, B. Cover systems and landforms for rehabilitation of mine waste storage facilities: Practical insights. *CIM J.* **12**, 60–70. https://doi.org/10.1080/19236026.2021.1919010 (2021).
19. Hudson-Edwards, K. A. et al. Tailings storage facilities, failures and disaster risk. *Nat. Rev. Earth Environ.* **5**, 612–630 (2024).

20. Ercikdi, B., Cihangir, F., Kesimal, A. & Deveci, H. in *Practical importance of tailings for cemented paste backfill*. 7–32 (eds Paste Tailings, M., Yilmaz, E. & Fall, M.) (Springer, 2017).
21. Yilmaz, E. & Fall, M. Introduction to paste tailings management. In Paste Tailings Management (eds (eds Yilmaz, E. & Fall, M.) 1–5 (Springer, Cham, (2017).
22. Koc, E., Cihangir, F., Ercikdi, B. & Deveci, H. Evaluation of acid mine drainage and metal release potential of cemented paste backfill of sulfide rich tailings. *Int. J. Min. Reclam. Environ.* **39**, 491–510. https://doi.org/10.1080/17480930.2024.2444885 (2025).
23. Liu, L. et al. Pore and strength characteristics of cemented paste backfill using sulphide tailings: Effect of sulphur content. *Constr. Build. Mater.* **237**, 117452. https://doi.org/10.1016/j.conbuildmat.2019.117452 (2020).
24. Yılmaz, T., Ercikdi, B. & Deveci, H. Evaluation of geochemical behaviour of flooded cemented paste backfill of sulphide-rich tailings by dynamic-tank leaching test. *Int. J. Min. Reclam. Environ.* **35**, 336–355. https://doi.org/10.1080/17480930.2020.1829778 (2021).
25. Benzaazoua, M., Belem, T. & Bussière, B. Chemical factors that influence the performance of mine sulphidic paste backfill. *Cem. Concr Res.* **32**, 1133–1144. https://doi.org/10.1016/S0008-8846(02)00752-4 (2002).
26. Benzaazoua, M. et al. Integrated mine tailings management by combining environmental desulphurization and cemented paste backfill: Application to mine Doyon, Quebec. *Can. Min. Eng.* **21**, 330–340. https://doi.org/10.1016/j.mineng.2007.11.012 (2008).
27. Mafra, C., Bouzahzah, H., Stamenov, L. & Gaydardzhiev, S. An integrated management strategy for acid mine drainage control of sulfidic tailings. *Min. Eng.* **185**, 107709. https://doi.org/10.1016/j.mineng.2022.107709 (2022).
28. Kongolo, M., Benzaazoua, M., Donato, P., Drouet, B. & Barres, O. The comparison between amine thioacetate and amyl xanthate collector performances for pyrite flotation and its application to tailings desulphurization. *Min. Eng.* **17**, 505–515. https://doi.org/10.1016/j.mineng.2004.01.003 (2004).
29. Richards, J. P. Tectonic, magmatic, and metallogenic evolution of the Tethyan orogen: From subduction to collision. *Ore Geol. Rev.* **70**, 323–345. https://doi.org/10.1016/j.oregeorev.2014.11.009 (2015).
30. Dokuz, A., Gücer, M. A., Karslı, O. & Yi, K. From Cadomian back-arc basin to Rheic Ocean closure: The geochronological records of the Kurtoğlu Massif, eastern Sakarya Zone, Turkey. *Int. J. Earth Sci.* **111**, 1333–1355. https://doi.org/10.1007/s00531-022-02183-4 (2022).
31. Topuz, G. et al. Carboniferous high-potassium I-type granitoid magmatism in the Eastern Pontides: The Gümüşhane pluton (NE Turkey). *Lithos* **116**, 92–110. https://doi.org/10.1016/j.lithos.2010.01.003 (2010).
32. Dokuz, A. A slab detachment and delamination model for the generation of Carboniferous high-potassium I-type magmatism in the Eastern Pontides, NE Turkey: Köse composite pluton. *Gondwana Res.* **19**, 926–944. https://doi.org/10.1016/j.gr.2010.09.006 (2011).
33. Kaygusuz, A., Arslan, M., Siebel, W., Sipahi, F. & İlbeyli, N. Geochronological evidence and tectonic significance of Carboniferous magmatism in the southwest Trabzon area, eastern Pontides, Turkey. *Int. Geol. Rev.* 1776–1800. https://doi.org/10.1080/00206814.2012.676371 (2012).
34. Karslı, O., Dokuz, A. & Kandemir, R. Subduction-related Late Carboniferous to Early Permian magmatism in the Eastern Pontides, the Camlik and Casurluk plutons: Insights from geochemistry, whole-rock Sr–Nd and in situ zircon Lu–Hf isotopes, and U–Pb geochronology. *Lithos* **266**, 98–114. https://doi.org/10.1016/j.lithos.2016.10.007 (2016).
35. Gücer, M. A. & Sarı, E. Karbonifer Pamuktaş Plütonu'nun petrografisi, jeokimyası ve petrolojik özellikleri, Bayburt (KD Türkiye). *Yerbilimleri* **42**, 85–120. https://doi.org/10.17824/yerbilimleri.889227 (2021).

36. Kandemir, R. & Yılmaz, C. Lithostratigraphy, facies and deposition environment of the Lower Jurassic Ammonitico Rosso type sediments (ARTS) in the Gumushane area, NE Turkey: Implications for the opening of the northern branch of the Neo-Tethys Ocean. *J. Asian Earth Sci.* **34**, 586–598. https://doi.org/10.1016/j.jseaes.2008.08.006 (2009).
37. Güven, İ. H. *Doğu Karadeniz Bölgesi'nin 1/25.000 Ölçekli Jeolojisi ve Kompilasyonu* (MTA, Ankara, 1993). (in Turkish).
38. Tüysüz, N. & Geology lithogeochemistry and genesis of the Murgul massive sulfide deposit, NE Turkey. *Chem. Erde*. **60**, 231–250 (2000).
39. Demir, Y., Uysal, İ., Sadıklar, M. B. & Sipahi, F. Mineralogy, mineral chemistry, and fluid inclusion investigation of Köstere hydrothermal vein-type deposit (Gümüşhane. *NE-Turkey) Neues Jahrb Mineral. Abh*. **185**, 215–232. https://doi.org/10.1127/0077-7757/2008/0122 (2008).
40. Demir, Y., Uysal, İ. & Sadıklar, M. B. Mineral chemical investigation on sulfide mineralization of the Istala deposit, Gümüşhane, NE-Turkey. *Ore Geol. Rev.* **53**, 306–317. https://doi.org/10.1016/j.oregeorev.2013.01.014 (2013).
41. Sipahi, F. et al. Eocene magmatism and associated Fe–Cu mineralization in northeastern Turkey: A case study of the Karadağ skarn. *Int. Geol. Rev.* **64**, 1530–1555. https://doi.org/10.1080/00206814.2021.1941323 (2022).
42. Sipahi, F., Sadıklar, M. B., Gücer, M. A., Aydın, A. & Kara, R. T. A study on the magnetite skarn mineralization (Gümüşhane, Türkiye): A magnetic survey. *Turk. J. Earth Sci.* **33**, 915–930. https://doi.org/10.55730/1300-0985.1882 (2023).
43. Sipahi, F., Zeybek, H. İ., Gücer, M. A. & Işık, F. Comparison with carbonate rocks hosted iron skarn in the eastern Sakarya Zone (Gümüşhane, NE Turkey): A geomorphologic, geochemical and stable isotopic approach. *Carbonates Evaporites*. **39**, 80. https://doi.org/10.1007/s13146-024-00991-0 (2024).
44. Sipahi, F. et al. Origin and tectonic setting of the carbonate-hosted Kopuz Fe skarn deposit, Sakarya Zone, NE Türkiye. *J. Asian Earth Sci.* **294**, 106769. https://doi.org/10.1016/j.jseaes.2025.106769 (2025).
45. Akaryalı, E. & Tüysüz, N. The genesis of the slab window-related Arzular low-sulfidation epithermal gold mineralization (Eastern Pontides, NE Turkey). *Geosci. Front.* **4**, 409–421. https://doi.org/10.1016/j.gsf.2012.12.002 (2013).
46. Akaryalı, E. & Akbulut, K. Constraints of C–O–S isotope compositions and the origin of the Ünlüpınar volcanic-hosted epithermal Pb–Zn ± Au deposit, Gümüşhane, NE Turkey. *J. Asian Earth Sci.* **117**, 119–134. https://doi.org/10.1016/j.jseaes.2015.12.012 (2016).
47. Akaryalı, E. Geochemical, fluid inclusion and isotopic (O, H and S) constraints on the origin of Pb–Zn ± Au vein-type mineralizations in the Eastern Pontides Orogenic Belt (NE Turkey). Ore Geol. Rev. 74, 1–14. (2016). https://doi.org/10.1016/j.oregeorev.2015.11.013
48. Arslan, M., Tüysüz, N., Korkmaz, S. & Kurt, H. Geochemistry and petrogenesis of the Eastern Pontide volcanic rocks, Northeast Turkey. *Chem. Erde Geochem.* **57**, 157–187 (1997).
49. Aslan, Z. U–Pb zircon SHRIMP age, geochemical and petrographical characteristics of tuffs within calc-alkaline Eocene volcanics around Gümüşhane (NE Turkey, Eastern Pontides). *Neues Jahrb Mineral. Abh*. **187**, 329–346. https://doi.org/10.1127/0077-7757/2010/0181 (2010).
50. Gücer, M. A., Aydınçakır, E., Yücel, C. & Akaryalı, E. Tersiyer yaşlı Altınpınar hornblendli andezitlerinin (Torul-Gümüşhane) petrografisi, mineral kimyası ve P–T kristalleşme koşulları. Gümüşhane Univ. *J. Sci. Technol.* **7**, 236–267. https://doi.org/10.17714/gumusfenbil.310263 (2017).
51. Gücer, M. A. & Origin petrogenesis and geodynamic implications of the early Eocene Altınpınar adakitic andesites in the eastern Sakarya Zone, northeastern Turkey. *Geochemistry* **81**, 1–21.

https://doi.org/10.1016/j.chemer.2021.125766 (2021).
52. Köprübaşı, N. Aşağı Harşit Bölgesinin Mağmatik Petrojenezi ve Masif Sülfitlerde Jeokimyasal Hedef Saptama Uygulamaları. PhD thesis, Karadeniz Technical University, Trabzon (in Turkish). (1992).
53. Republic of Türkiye. Regulation on Surface Water Quality Management. Official Gazette No. 28483. revised by Official Gazette No. 29327 (2015). (2012).
54. Ficklin, W. H., Plumlee, G. S., Smith, K. S. & McHugh, J. B. Geochemical classification of mine drainages and natural drainages in mineralized areas. In Proceedings of the 7th International Water–Rock Interaction Conference (eds Kharaka, Y. K. & Maest, A. S.) 381–384Balkema, Rotterdam, (1992).
55. Plumlee, G. S. et al. Park City, Utah,. Geological and geochemical controls on the composition of mine drainages and natural drainages in mineralized areas. In Proceedings of the 7th International Water–Rock Interaction Conference 419–422 (1992).
56. Plumlee, G. S. et al. Society of Economic Geologists, Littleton,. Geologic controls on the composition of natural waters and mine waters draining diverse mineral-deposit types. In The Environmental Geochemistry of Mineral Deposits. Part B: Case Studies and Research Topics, Vol. 6B (eds Filipek, L. H. & Plumlee, G. S.) 373–432 (1999). https://doi.org/10.5382/Rev.06.19
57. Price, W. A., Errington, J. & Koyanagi, V. Guidelines for the prediction of acid rock drainage and metal leaching for mines in British Columbia: Part I. General procedures and information requirements. In Proceedings of the 4th International Conference on Acid Rock Drainage (ICARD) 1, 1–14Natural Resources Canada, Ottawa, (1997).
58. Ferguson, K. D. & Morin, K. A. The prediction of acid rock drainage—lessons from the database. In Proceedings of the 2nd International Conference on Acid Rock Drainage (ICARD) 83–106 (Montréal, Canada, 1991).
59. Brodie, M. J., Broughton, L. M. & Robertson, A. A conceptual rock classification system for waste management and a laboratory method for ARD prediction from rock piles. In Proceedings of the 2nd International Conference on Acid Rock Drainage (ICARD) 3, 119–135 (1991).
60. Sobek, A. A., Schuller, W. A., Freeman, J. R. & Smith, R. M. *Field and Laboratory Methods Applicable to Overburdens and Minesoils. EPA-600/2-78-054* (U.S. Government Printing Office, 1978).

Figures

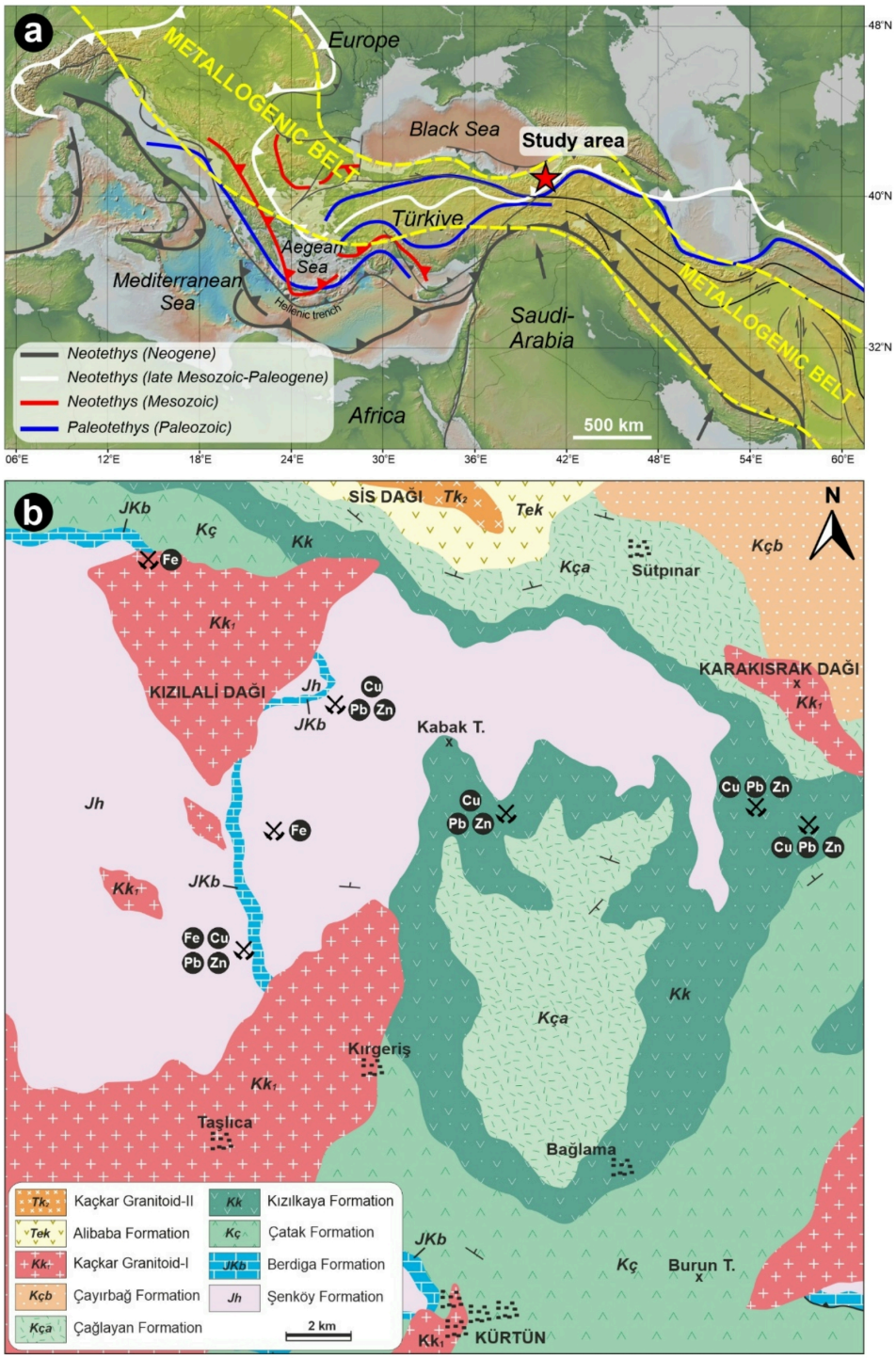


Figure 1

(a) The main tectonic structures of Türkiye and the surrounding area, including the metallogenic belt (modified after **29**). **(b)** Detailed geological maps of the study area

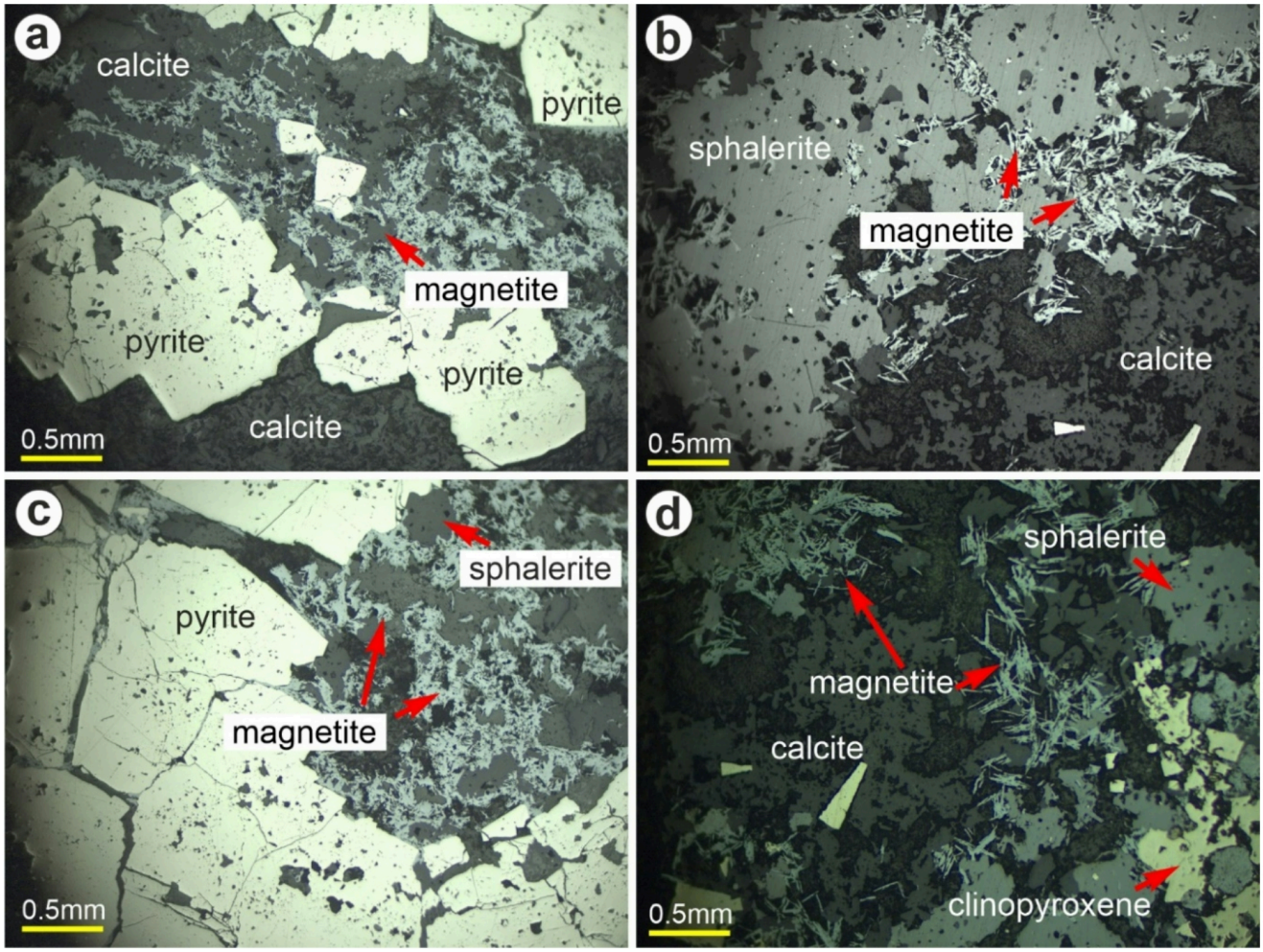


Figure 2

Representative microscopic images of ore mineral assemblages from the study area, showing pyrite, sphalerite, magnetite, calcite, and clinopyroxene.

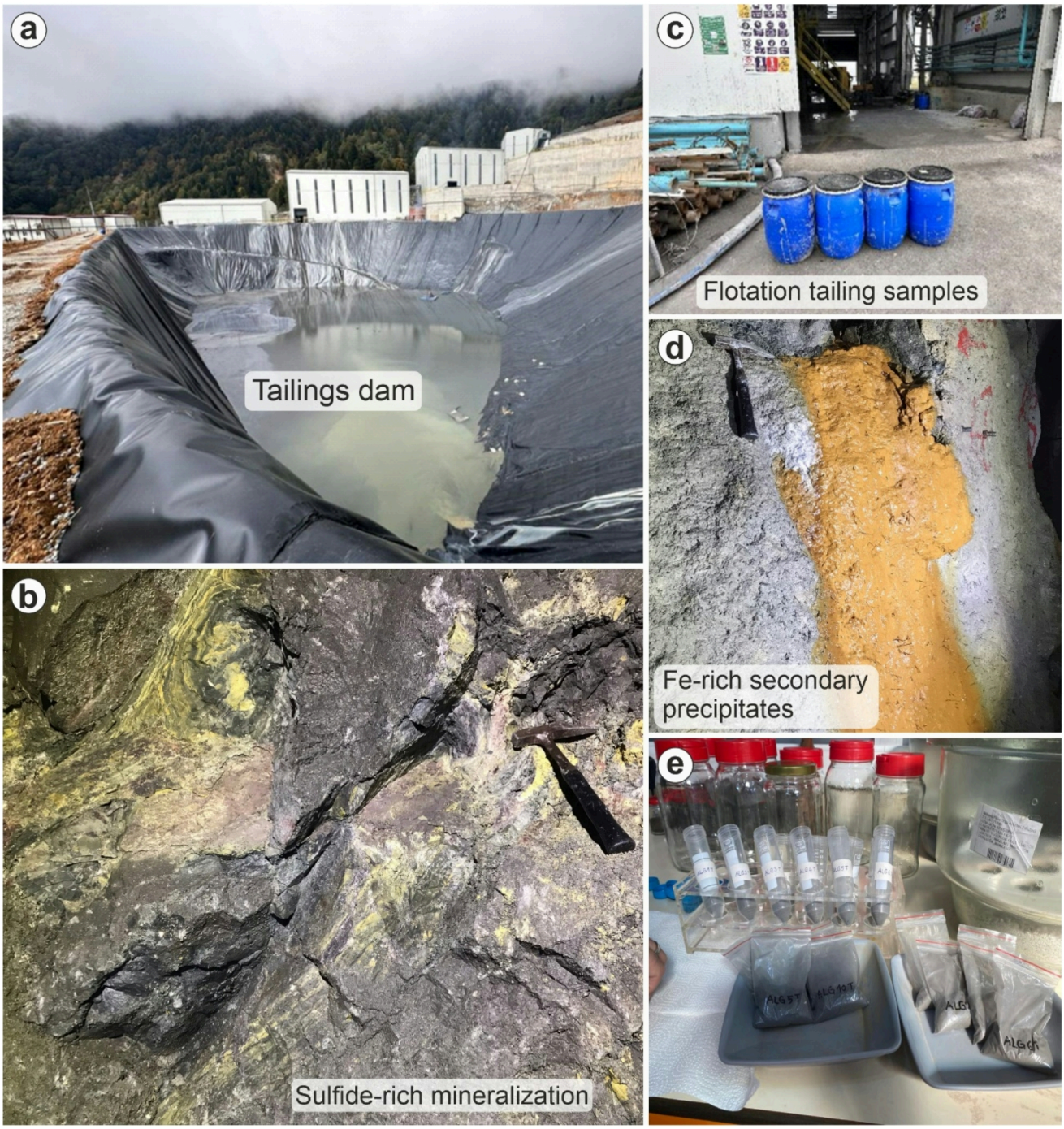


Figure 3

Representative field observations and materials used in this study. (a) tailings storage facility, (b) sulfide-rich mineralization in an underground gallery, (c) flotation tailing samples, (d) Fe-rich secondary precipitates related to sulfide oxidation, and (e) laboratory-prepared samples for mineralogical, geochemical, and AMD analyses.

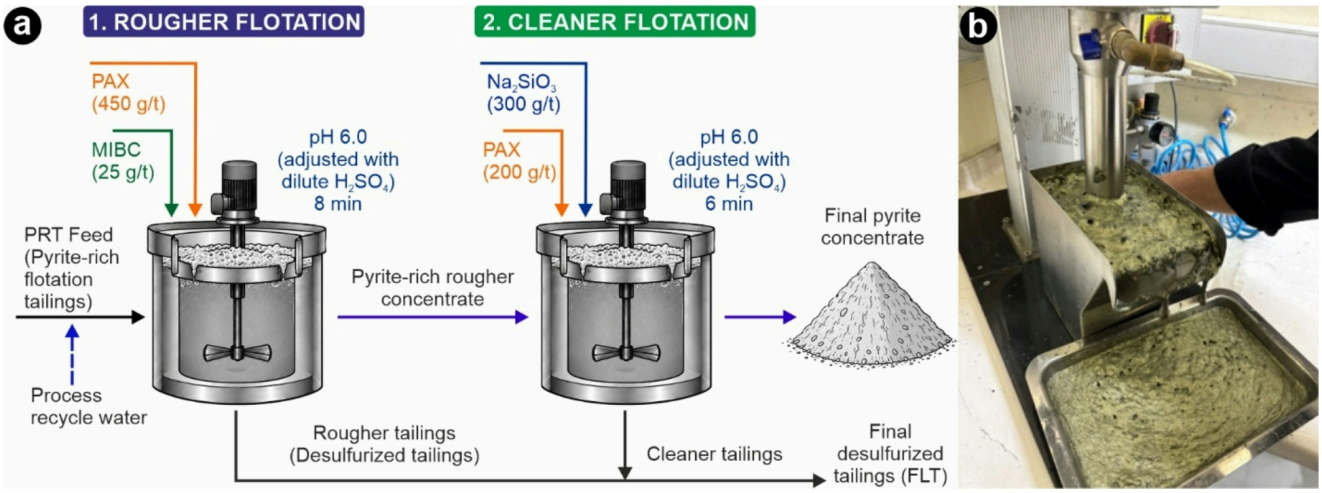


Figure 4

Selective pyrite flotation process. **(a)** schematic illustration of the two-stage rougher-cleaner flotation circuit used to produce the final pyrite concentrate and desulfurized flotation tailings (FLT), and **(b)** representative laboratory-scale pyrite flotation experiment.

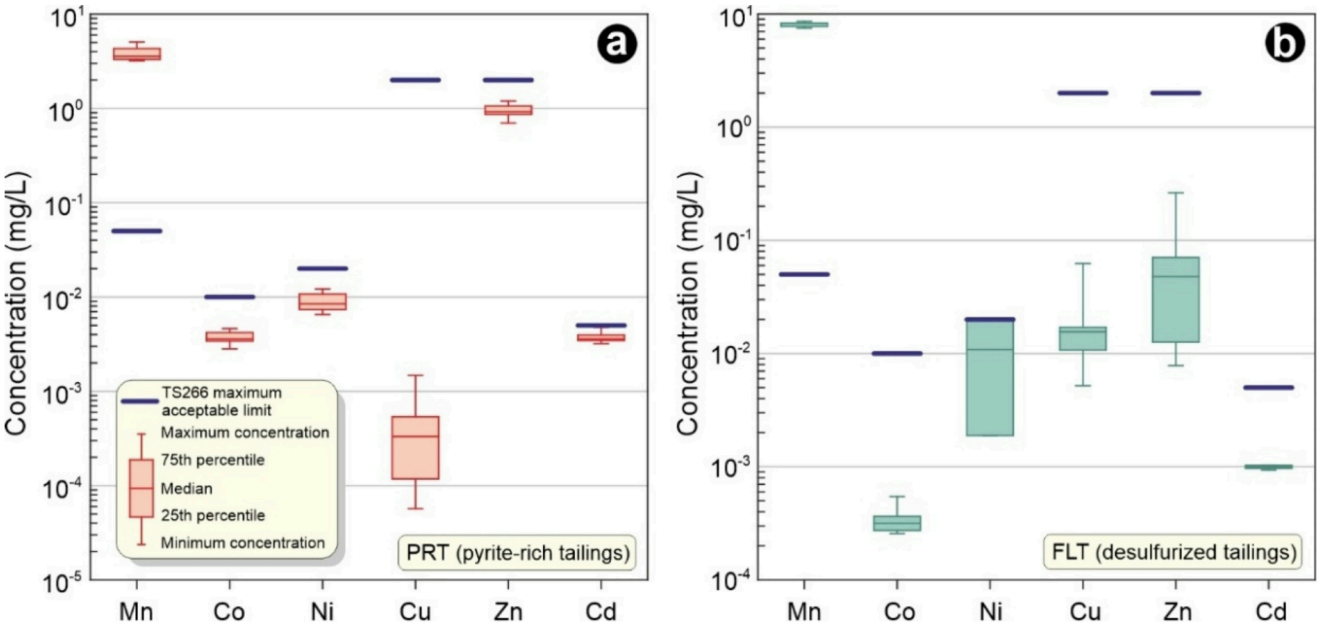


Figure 5

Boxplots showing summary statistics for selected potentially toxic element concentrations in filtered leachates from **(a)** PRT and **(b)** FLT samples, compared with the maximum acceptable limits of TS266.

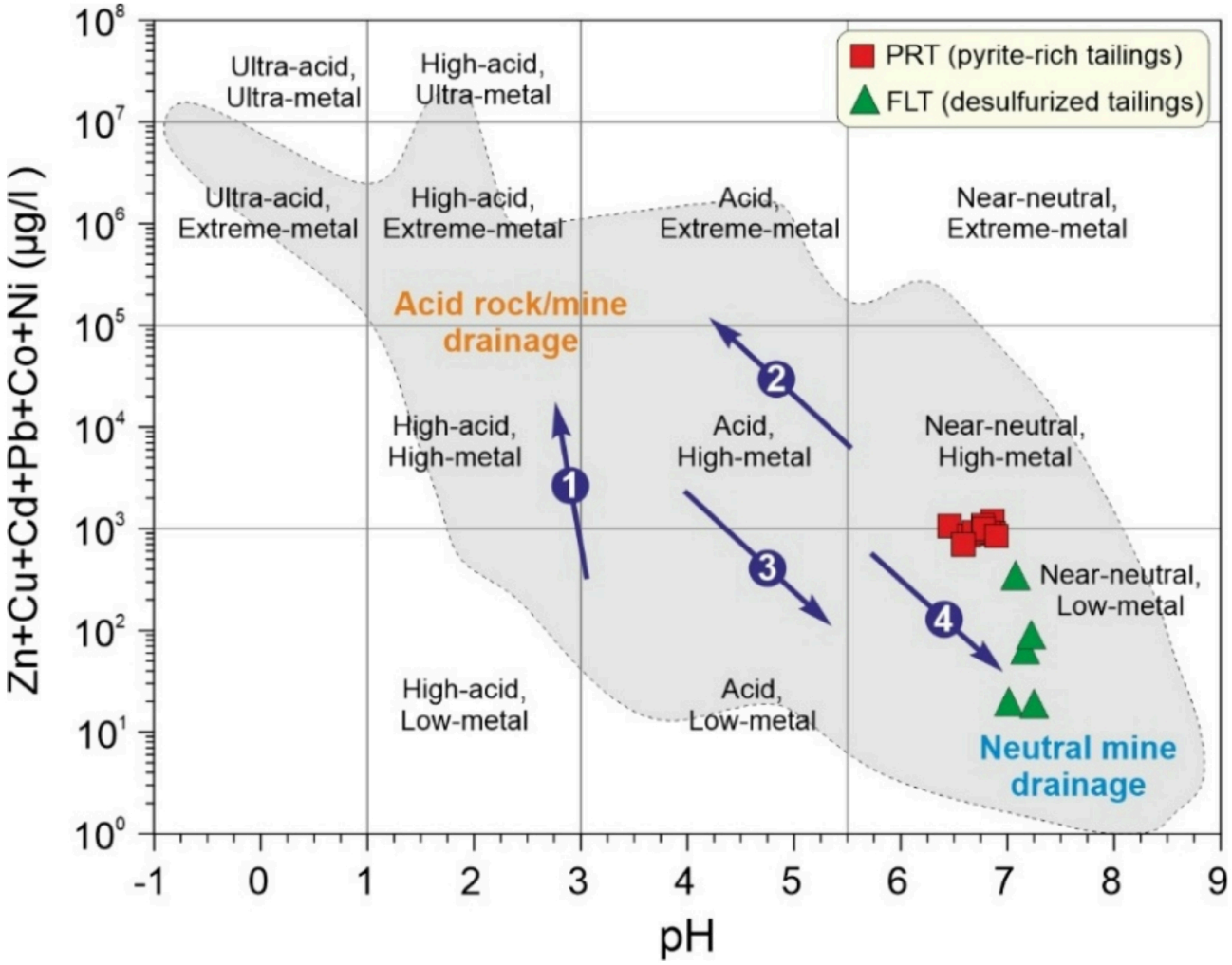


Figure 6

Ficklin geochemical classification diagram showing the distribution of PRT and FLT leachates. Numbered arrows indicate the principal controls on mine-drainage chemistry: (1) increasing base-metal sulfide content, (2) increasing pyrite content, (3) increasing carbonate content, and (4) increasing dilution by surface water. Classification fields are based on (**54**) and (**55-56**) and grey area adapted from (**56**).

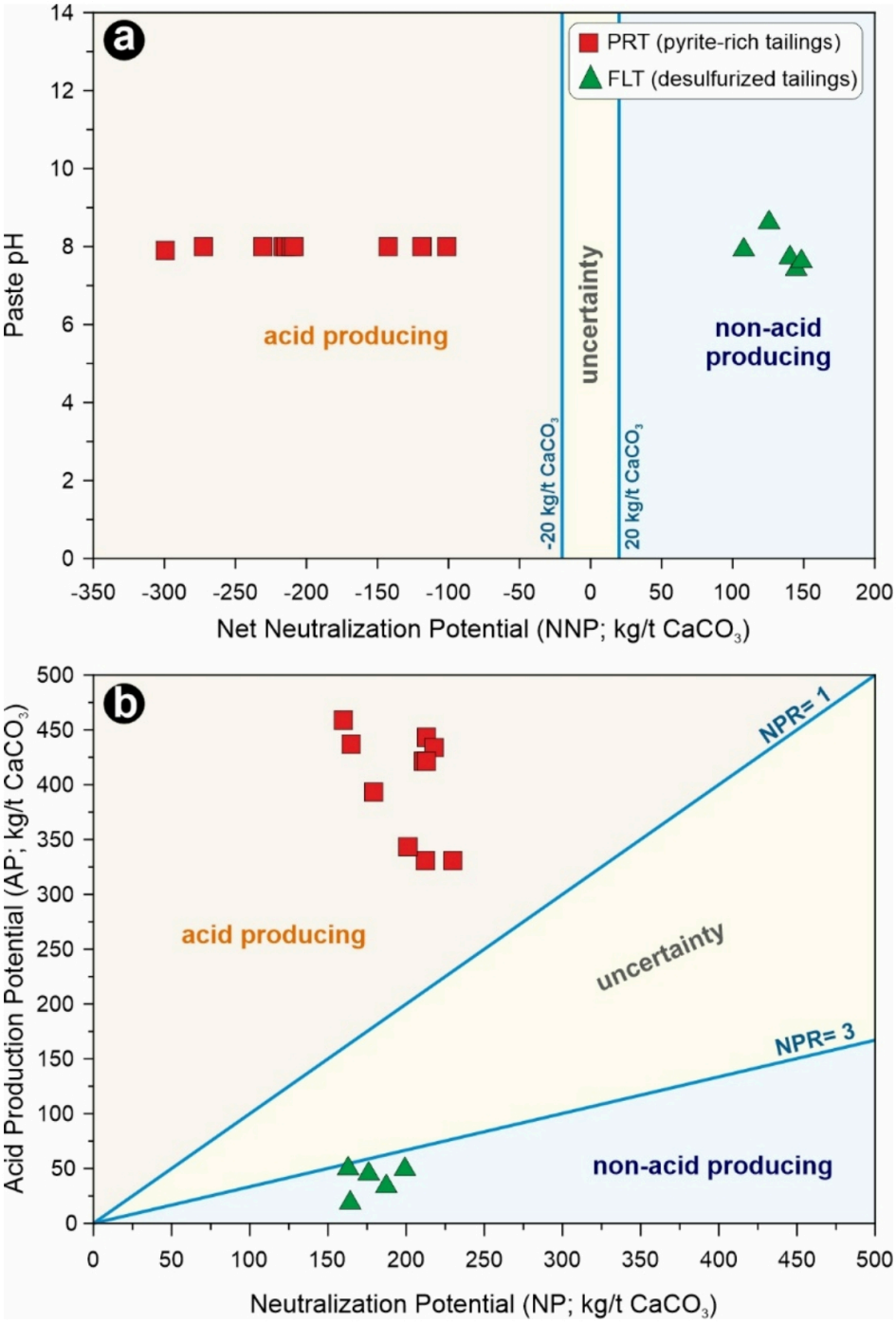


Figure 7

Classification of the acid-generation potential of PRT and FLT samples based on acid-base accounting parameters. **(a)** Paste pH vs Net Neutralization Potential (NNP) and **(b)** Acid Potential (AP) vs Neutralization Potential (NP). Classification criteria are based on (**58-59**), respectively.

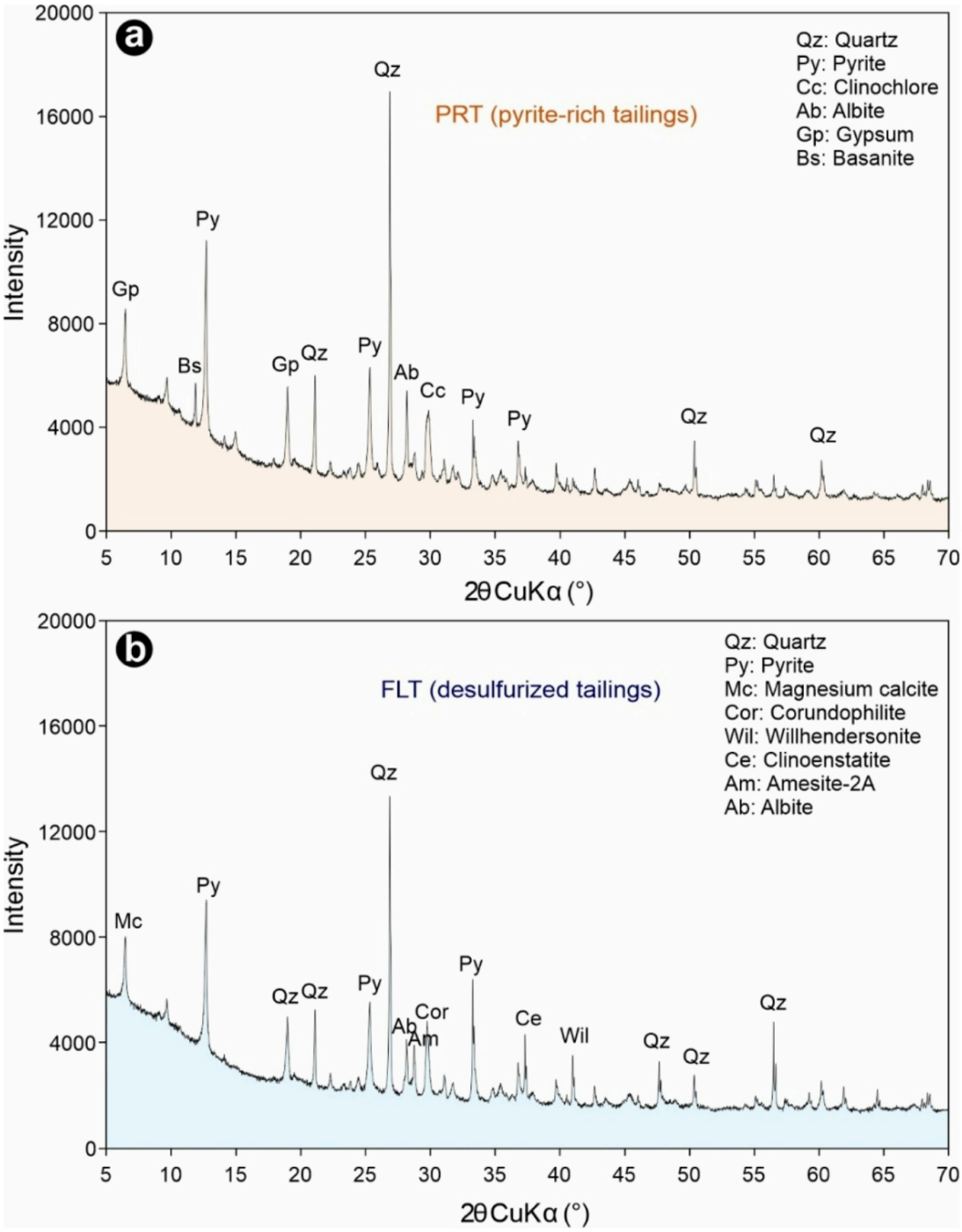


Figure 8

X-ray diffraction (XRD) patterns of **(a)** pyrite-rich flotation tailings (PRT) and **(b)** desulfurized flotation tailings (FLT), illustrating the mineralogical changes associated with selective pyrite removal.